ELEKTROTEHNIŠKI VESTNIK 85(1-2): 62-68, 2018
ORIGINAL SCIENTIFIC PAPER

Magnetic Field Analysis of a Compound-drive-type Multi-degree-of-freedom Permanent-magnet Motor with a Liquid Suspension Mode

Zheng Li[1], Shuanghong Li[1], Ruodong Zhi[1], Guangjing Su[2], Zhe Qian[3], Qunjing Wang[3]

[1]School of Electrical Engineering, Hebei University of Science and Technology, Shijiazhuang 050018, China;
[2]School of Electrical Engineering and Automation, Hefei University of Technology, Hefei 230009, China;
[3]National Engineering Laboratory of Energy-saving Motor & Control Technique, Anhui University, 230039 Hefei, China
E-mail: Lzhfgd@163.com

Abstract. The paper proposes a compound-drive-type multi-degree-of-freedom permanent-magnet motor with a liquid-suspension mode. The basic structure and working principle of the motor are introduced and a method to calculate the air-gap magnetic field of the permanent-magnet motor for the imposed motor is presented. The air-gap magnetic field is analyzed by using an analytical method and finite-element method. A Comparison and validation of results are accomplished. A model is brief of the permanent-magnet magnetic field, making a comparison between changes resulting from eccentric and noneccentric motor states and results are given of analyzing harmonic components at different air-gap lengths. The results validate of the motor structure design, thus providing a theoretical basis for further study of this kind of motors.

Keywords: compound drive; multi-degree-of-freedom; air-gap magnetic field; eccentric magnetic field

Analiza magnetnih polj večdimenzionalnega tekočinsko dušenega pogona s trajnimi magneti

V članku predstavljamo analizo magnetnih polj večdimenzionalnega tekočinsko dušenega pogona s trajnimi magneti. Podrobno smo predstavili zgradbo pogona in njegovo delovanje. S predlagano zgradbo pogona smo opisali tudi metodo za izračun magnetnega polja za tovrstne pogone. Z metodo končnih elementov smo analizirali magnetno polje v zračni reži. Zgradili smo model za magnetno polje pri rotorju s trajnimi magneti za primer ekscentričnost in ga preverili pri različnih dolžinah zračne reže. Rezultati potrjujejo veljavnost predlagane zgradbe pogona in predstavljajo teoretično osnovo za nadaljnje raziskave.

1 INTRODUCTION

In the traditional multi-degree-of-freedom systems, two or more single-degree-of-freedom motors are usually used to complete complex multidimensional motions. Usually, these systems use a large number of reduction gears to increase the volume of the system and reduce the stiffness. Meanwhile, affected by the derivative nonlinear friction and other factors, the control system hardly derives a satisfactory dynamic performance and has a relatively long response time. Stability of the motion system may also get worse. Besides, the magnetic field of a traditional multi-degree-of-freedom motor is not easy to be controlled, which greatly affects its operation mode and control accuracy. The traditional mechanical bearing mechanism used by the multi-degree-of-freedom motor has some disadvantages, such as friction loss and low motion stability, which results in limited applications of the motor. The current compound-drive-type motors also have some disadvantages, including the complex stator iron core and complicated windings, which have not got enough attention. The mechanical bearing-friction resistance affects the dynamic characteristics of the rotor that causes poor efficiency and shortened the lifetime of the motor. Meanwhile, the multi-degree-of-freedom permanent-magnet motor has been on increasing affection for its achieving a spacial movement with no complicated excitation device and for its small size and simple structure.

The paper presents a compound-drive-type multi-degree-of-freedom permanent-magnet motor with a liquid suspension mode. The liquid bearing effectively reduces the loss caused by friction, prolongs its service life and greatly improves the control precision.

2 STRUCTURE AND WORKING PRINCIPLE OF THE MOTOR

2.1 The basic structure of the motor

The motor mainly consists of three components, the stator spherical shell, spherical rotor and output shaft. The outer stator spherical shell is inlaid with windings.

Received 9 February 2017
Accepted 5 January 2018

There are six pairs of coils for a large-scale rough-control mode. They are distributed in two layers. Each pair of the control coils has a 60-degree difference on the space and each layer of the control coils has 50-degree a difference on the space. The middle line of the control coils crosses the center point of the permanent-magnet rotor. For a small-scale fine adjustment, the coil system with its iron cores cross-shaped is placed at the end of the stator spherical shell. Five windings are oriented on the stator core. Inside the rotor spherical shell, there are two pairs of a large-scale rough-adjustment permanent magnet with the N and S poles alternatively distributed. The permanent magnet for a fine-adjusment control is placed on the rear. The output shaft of the motor is fixed on the permanent magnet so that there is a linkage between the rotor and the output shaft. In order to reduce the friction caused by the rotor motion, the liquid bearing is sealed between the stator spherical shell and the rotor. A model of the motor structure with its stator spherical shell and spherical rotor is shown Fig.1. The main structure parameters of the motor model are given in Table 1.

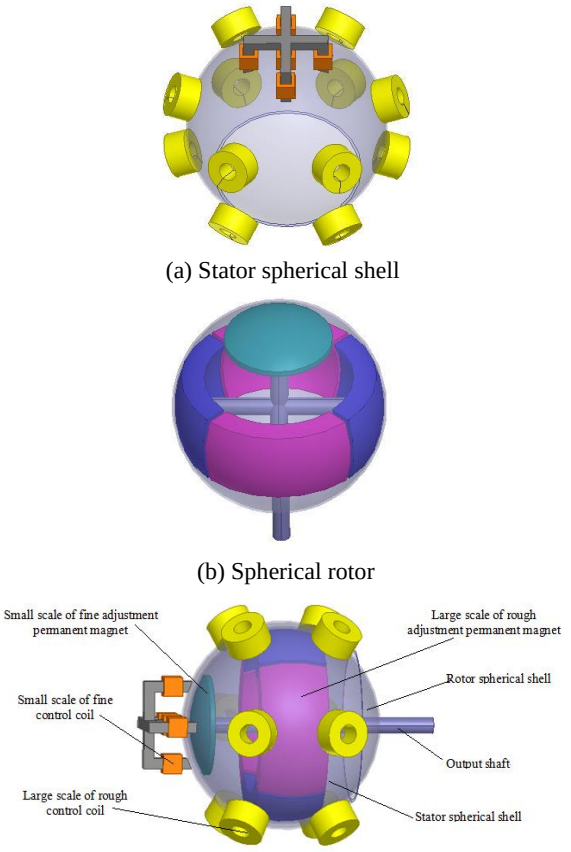

(a) Stator spherical shell

(b) Spherical rotor

(c) Integrated model

Figure 1. Structure of the motor

Table1. Main structure parameters of the motor

Parameters	Value
Motor height	69mm
Outer diameter of the stator spherical shell	55mm
Outer diameter of the bipolar permanent magnet	50mm
Inner diameter of the bipolar permanent magnet	38mm
Outer diameter of the single-pole permanent magnet for fine motion control	26mm
Fluid thickness	3mm
Rotor shell thickness	1mm

2.2 The working principle of the motor

When the stator coils are activated with currents, there will be an interaction between the magnetic field caused by the coils and the large-scale adjustment permanent magnets, producing the tangential and radial forces. The radial component of the electromagnetic force cannot generate a torque, but can change the stator displacement. Meanwhile, the tangential force makes the motor rotate and deflect. By tracking and controlling the amplitude and direction of the stator-coil currents that are located in different positions, the rotor can be implemented so as to deflect at a large-scale motion. After a large-scale deflection angle, the ending small-scale fine- adjustment coils need to be adjusted. And by activating the coils with currents of given a direction and amplitude, the air-gap magnetic circuit will change, making the rotor to perform have a small-scale deflection movement. Thus, the motor can move to a precise position by changing and combining currents in different coils. In short, a compound-drive motion can be achieved by combining a large-scale deflection movement with a small-scale fine movement.

First, the large-scale movement of the motor will be discussed. As shown in Fig. 2, there are six pairs of the large-scale adjustment coils and permanent magnets. By electrifying C, D, A'and F' with currents of the same direction and same amplitude, the N pole can be obtained, and by charging C', D', A and F with currents of the opposite direction and of the same amplitude, the generated magnetic pole is the S pole. Thus the tangential force made by the reaction between the coils and the permanent magnets can rotate the rotor around the X axis. Likewise, the motor can deflect its motion around the Y axis by a force generated by the N and S magnetic poles when activating the E and B' coils as well as the E' and B coils. Using the same electrifying strategy, the motor will rotate around the Z axis when the C, C', F and F' coils and the D, D', A and A' coils are activated. In this way, the motor makes a multi-degree-of-freedom motion around the X, Y and Z axis by controlling different coils.

In the next step, a fine movement of the motor is now exerted. The fine-control coils are labeled with *a*, *b*, *c*, *d*, *e*. Fig. 3 shows the relative positions of the permanent magnet at the bottom and fine-control coils when the motor rotate around the X axis. By activating the *b* and

d fine-control coils with the currents of different directions and of the same amplitudes, the S and N pole will be obtained, and the motor will be rotating around the X axis continually with a small angle. To achieve a fine movement and deflection in all directions according to different moving angles, the different fine-adjustment coils need to be implemented together.

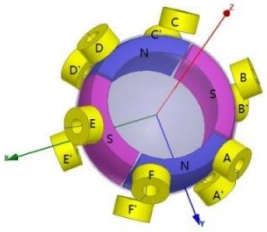

Figure 2. Large-scale rough-control principle

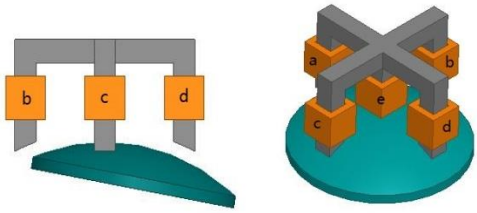

Figure 3. Small-scale fine-control principle

3 Analytical Method of the Motor Magnetic Field

3.1 Magnetic field regions

With a fluid suspension in the motor structure and using different magnetic media in different regions with different boundary conditions, the magnetic field is divided into four regions:

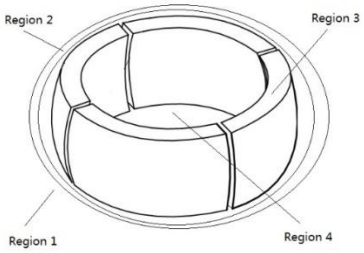

Figure 4. Magnetic-field regions

(1) Region 1: the outer air-gap magnetic-field characteristic of the stator spherical shell is

$$B_1 = \mu_0 H_1 \tag{1}$$

where μ_0 is approximately equal to the vacuum permeability of $4\pi\times10^{-7}\,H/m$.

(2) Region 2: the magnetic-field characteristic between the rotor and the stator spherical shell in the bearing liquid region is:

$$B_2 = \mu_0\mu_k H_2 \tag{2}$$

where μ_k is the relative permeability of the fluid.

(3) Region 3: the inner magnetic field of the rotor permanent-magnet magnetic poles is:

$$B_3 = \mu_0\mu_r H_3 + \mu_0 M_0 \tag{3}$$

Where, μ_r =1.02 is the relative permeability of the rotor poles; and $M_0 = B_0/\mu_0$ is the residual magnetization. The residual magnetization of the permanent magnets can be expressed as:

$$M_0 = \begin{pmatrix} M_{(0,\gamma)} \\ M_{(0,\theta)} \\ M_{(0,\varphi)} \end{pmatrix} = (-1)^{p-1}|M_0| \begin{pmatrix} \cos(\varphi-\alpha_p)\sin\theta \\ \cos(\varphi-\alpha_p)\cos\theta \\ -\sin(\varphi-\alpha_p) \end{pmatrix} \tag{4}$$

where $\alpha_p = \frac{\alpha}{2} + 2\pi\frac{p-1}{p}$, $0 < \varphi - 2\pi\frac{p-1}{p} < \alpha$,

So, the inequalities of φ, θ are:

$$2\pi\frac{p-1}{p} < \varphi < \alpha + 2\pi\frac{p-1}{p} \tag{5}$$

$$\frac{\pi}{2} - \frac{\beta}{2} < \theta < \frac{\pi}{2} + \frac{\beta}{2} \tag{6}$$

(4) Region 4: the inter rotor magnetic field is:

$$B_4 = \mu_0\mu_m H_4 \tag{7}$$

In this formula, relative permeability $\mu_m = 1$.

As there are no excitation currents in regions 1, 2, 3 and 4 of the rotor permanent magnet, the magnetic-field equations for the four regions can be expressed as:

$$\nabla\times H_k = 0\,; \quad \nabla\bullet B_k = 0 \tag{8}$$

where the *k* value is 1, 2, 3, 4.

So, the relationship between scalar magnetic potential φ_k gradient and magnetic-field strength H_k is :

$$H_k = -\nabla\varphi_k \tag{9}$$

The Laplace's equation of the scalar magnetic potential for the four regions is :

$$\nabla^2\phi_1 = 0 \tag{10}$$

$$\nabla^2\phi_2 = \frac{1}{\mu_0\nabla\bullet M_0} \tag{11}$$

$$\nabla^2\phi_3 = 0 \tag{12}$$

As the magnetic field of the motor rotor part is symmetrically distributed over the entire space, $\nabla M_r = 0$.

3.2 Solving the Laplace's equation

As the motor is operated by a three-degree-of-freedom movement in the space, the spherical coordinate is used to solve the Laplace's equation. In the spherical coordinates,

$$\frac{1}{r^2}\left[\frac{\partial}{\partial r}(r^2\Phi_j) + \frac{1}{\sin\theta}\frac{\partial}{\partial\theta}(\sin\theta\frac{\partial\Phi_j}{\partial\theta}) + \frac{1}{\sin^2\theta}\frac{\partial\Phi_j}{\partial\varphi}\right] = 0 \tag{13}$$

The method of separating the variables is used to reduce the number of the unknown variables

$$z(r,\theta,\varphi) = R(r)W(\theta,\varphi) \tag{14}$$

Substituting r^2/z into equation, a general solution of the equation can be obtained by:

$$R(r) = A_n^m r^n + B_n^m \frac{1}{r^{n+1}} \tag{15}$$

The general solution for the scalar magnetic potential is:

$$\Phi = \sum_{n=0}^{\infty}\sum_{m=-n}^{n}(A_{n,j}^m r^n + B_{n,j}^m \frac{1}{r^{n+1}})W_n^m(\theta,\varphi) \tag{16}$$

where A_n^m and B_n^m are the unknown parameters, determined by the specific boundary conditions, $j=1,2$ are the two parts of the magnetic field and $W_n^m(\theta,\varphi)$ is the associated Legendre's function expressed as:

$$W_n^m(\theta,\varphi) = Q_n^m P_n^m(\cos\theta)e^{im\varphi} \tag{17}$$

$$Q_n^m = \sqrt{\frac{2n+1(n-|m|)!}{4\pi(n+|m|)!}} \tag{18}$$

$$P_n^m = \frac{1}{2^n n!}(1-y^2)^{\frac{m}{2}}\frac{d^{m+n}}{dx^{m+n}}(y^2-1)^n \tag{19}$$

$$e^{im\varphi} = \cos(m\varphi) + i\sin(m\varphi) \tag{20}$$

3.3 Solving the air-gap magnetic- flux density

Simplifying the solution, by setting up the specific boundary conditions of the magnetic field, then the general solution and special solution of Laplace equation are obtained.

The four regions of the spherical space in different setting conditions are needed in different magnetic fields. Together with A_n^m and B_n^m, here are eight unknown variables.

(1) In the outer region of the permanent-magnet rotor:

$$B_{1r} = B_{1\varphi} = B_{1\theta} = 0$$

The magnetic induction intensity is 0.

(2) For the junction of the stator spherical shell and liquid region, for the boundary between the liquid region and permanent magnet outer radius, and for the interface of the permanent-magnet inner radius with the rotor core, the expressions are:

$$B_{1r} = B_{2r}, H_{1\varphi} = H_{2\varphi}, H_{1\theta} = H_{2\theta}$$

$$B_{2r} = B_{3r}, H_{2\varphi} = H_{3\varphi}, H_{2\theta} = H_{3\theta}$$

$$B_{3r} = B_{4r}, H_{3\varphi} = H_{4\varphi}, H_{3\theta} = H_{4\theta}$$

(3)According to the magnetic-field, the flux density in the center of the magnetic field is:

$$B_{4r} = B_{4\theta} = B_{4\varphi} = \infty$$

By setting the boundary conditions, the air-gap flux density is obtained by :

$$B_{1r} = \sum_{n=0}^{\infty}\sum_{m=-n}^{n}[(n+1)\mu_r K_n^m \frac{1}{r^{n+2}}]Y_n^m(\theta,\varphi) \tag{21}$$

$$B_{1\theta} = \sum_{n=0}^{\infty}\sum_{m=-n}^{n}(-\mu_r K_n^m \frac{1}{r^{n+2}})\frac{\partial Y_n^m}{\partial\theta} \tag{22}$$

$$B_{1\varphi} = \sum_{n=0}^{\infty}\sum_{m=-n}^{n}(-\mu_r K_n^m \frac{1}{r^{n+2}})\frac{1}{\sin\theta}\frac{\partial Y_n^m(\theta,\varphi)}{\partial\theta} \tag{23}$$

From the above expressions, the air-gap magnetic field is divided into three fields, the radial magnetic field B_{1r}, the latitude direction magnetic field $B_{1\theta}$ and the longitude direction magnetic field $B_{1\varphi}$. The above three expressions of the air-gap flux density expression contain both the fundamental and harmonic components. The existence of harmonic components interfere with the normal distribution of air-gap magnetic field which effect to a certain extent also the magnetic-field strength. So the analysis and solution here only relate to the fundamental component of the magnetic field. The three-dimensional distribution characteristic of the air-gap magnetic field is shown in Figs. 5-7.

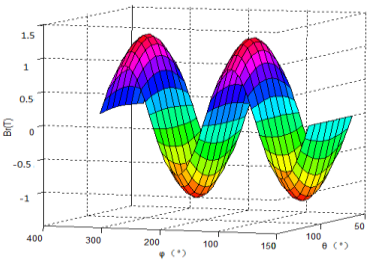

Figure 5. Three-dimensional distribution of B_{1r}

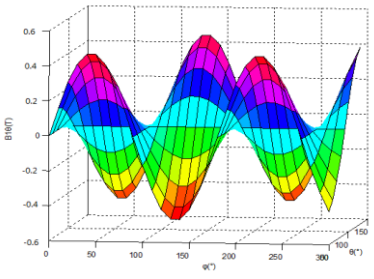

Figure 6. Three-dimensional distribution of $B_{1\theta}$

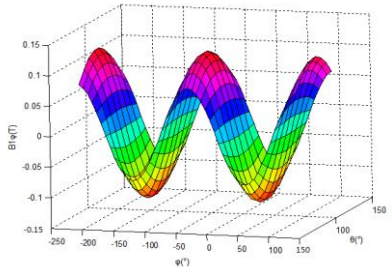

Figure 7. Three-dimensional distribution of $B_{1\varphi}$

In the distribution of the air-gap flux density shown in Fig. 5, B_{1r} is characterized by the cosine curves along abscissa φ, when considering the fundamental radial component. In a large-scale adjustment of the permanent magnets , there are two pole-pairs (P = 2), so there are two maximum and two minimum points in the outer circle of the rotor. The values are 1.47T and -1.47T, respectively. Fig. 5 shows that there are eight maximum points. Besides, when $\theta=0^{\circ}$, $\theta=90^{\circ}$, $\theta=180^{\circ}$ and $\theta=270^{\circ}$, the value of $B_{1\theta}$ is 0. As seen from Fig. 6, the trend of $B_{1\varphi}$ is similar to that of B_{1r} , which is characterized by the sine curves along abscissa φ. There are also two maximum and two minimum points in the outer circle of the rotor. The values are 0.12T and -0.12T, respectively. Among the three components of the air-gap flux density, the B_{1r} amplitude is the highest, the $B_{1\varphi}$ amplitude is the lowest, while the $B_{1\theta}$ amplitude is between the two amplitudes. The results of the analytic method clearly show the distribution and characteristics of the air-gap magnetic field.

4 FINITE ELEMENT ANALYSIS OF THE MOTOR

A 3D finite-element-analysis software is used to model a compound-drive-type multi-degree-of-freedom permanent-magnet motor with a liquid suspension mode. The solution region is twice of the model region. The model generating the mesh of the rotor permanent magnet is shown in Fig. 8.

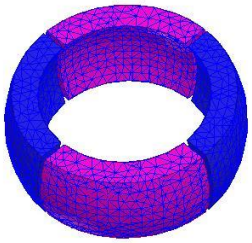

(a) Large-scale rough-adjustment permanent magnet

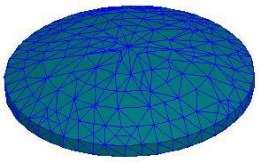

(b) Small-scale fine-adjustment permanent magnet

Figure 8. Mesh generation of the permanent magnet

Radial magnetizing direction of the permanent magnet is shown in Fig. 9. There is a closed magnetic-flux loop of the permanent-magnet air-gap flux density from the N to the S pole.

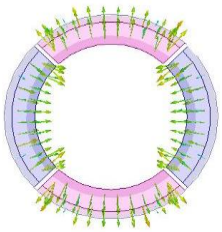

(a) Large-scale rough-adjustment permanent magnet

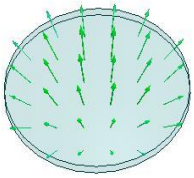

(b) Small-scale fine-adjustment permanent magnet

Figure 9. Radial-magnetizing flux-density vector distribution

Fig. 10 shows the distribution of the magnetic field density. As seen, the magnetic-field density of the permanent magnet at the borders is the strongest and at the pole is the weakest.

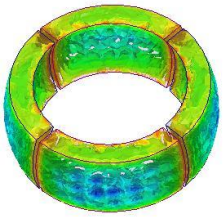

(1) Large-scale rough adjustment permanent magnet

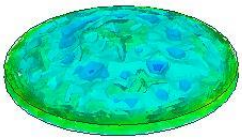

(2) Small-scale fine-adjustment permanent magnet

Figure 10. Distribution of the magnetic induction strength

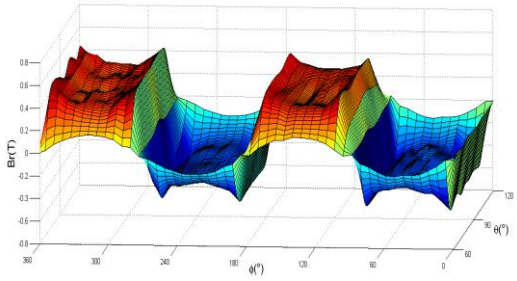

Figure 11. 3D space distribution of Br

In spherical coordinates, Fig. 11 shows a three-dimensional distribution of the air-gap flux density along the radial direction. Harmonics make the distribution of the air-gap flux density rectangular and the surface is no longer smooth. There are two maxima

and two minima in a cycle which coincides with the four-pole permanent- magnet structure. Validity of the analysis is verified.

5 Analysis of the Motor Eccentric Motion

5.1 Analysis of the eccentric air-gap magnetic field of the rotor

The motor is usually analyzed with its stator and rotor axes coinciding and the motor air-gap evenly distributed. When the rotor is eccentric, there will be a direct impact on the air-gap length of the motor making the motor air-gap unevenly distributed and generating on unbalanced magnetic-pull force. The mechanical loss of the motor may get increased and the circulating currents generated by the stator windings increase the electromagnetic power loss.

In order to get the air-gap flux density and the air-gap lengths, the first step is to derive the air-gap length formula. Fig. 12 shows the air-gap length coordinate system with a rotor eccentric motion. Fig. 13 is a projection of the sphere center on the plane, where R_s is the outer diameter of rotor permanent magnet, R_d is the inner diameter of the stator coil, O_s is the center of the sphere coordinate when the rotor is not eccentric, O_b is the center of the sphere coordinate when the rotor is eccentric. According to the geometric relationship, the expression of the air-gap length is:

$$l = \left[\Delta x \sin(\varphi) + \Delta y \cos(\varphi)\right]\sin(\theta) + \Delta z \cos(\theta) \quad (24)$$

where φ is the angle between the rotor sphere center and the X axis on the surface of XOY, θ is the angle between the rotor-sphere center and the Z axis when the rotor is eccentric. l_0 is defined as the air-gap length with no rotor eccentric motion, so the expression of the air-gap length with the rotor eccentric motion is:

$$l' = l_0 - l \quad (25)$$

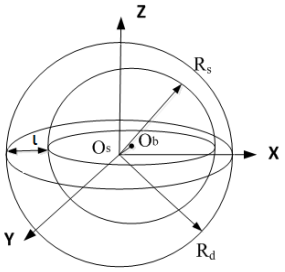

Figure 12. Air-gap coordinate of the rotor eccentricity

Without considering the impact of the harmonic components on the air-gap magnetic field, the distribution of the rotor eccentricity flux density can be obtained by using the air-gap flux-density expressions with no eccentric motion and the air-gap length formula based on the rotor eccentricity. The results are shown in Figs. 14-16.

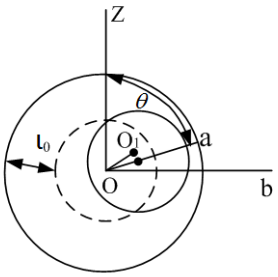

Figure 13. Rotor spherical center projection diagram

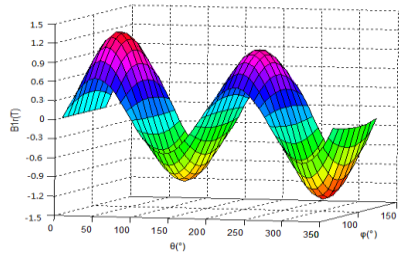

Figure 14. Eccentric radial flux-density distribution

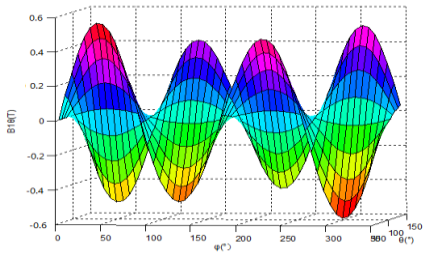

Figure 15. Eccentric flux-density distribution along the θ direction

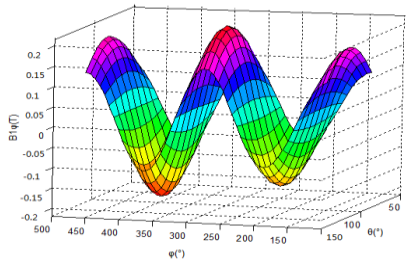

Figure 16. Eccentric flux-density distribution along the φ direction

As seem from Figs. 5-7, in a situation where the rotor is not eccentric, the magnetic-flux density on both sides of the rotor is evenly distributed and the distribution of the air-gap flux density follows the sine and cosine curves. Figs. 14, 15 and 16 are the air-gap flux-density distribution when the rotor is eccentric. As shown, the air-gap flux density is unevenly distributed on both sides of the rotor. On the side with the air-gap flux-density reduced, the magnitude of the flux density is greater than the magnitude of a noneccentric rotor. However, on the side of the increased air-gap flux

density, the magnitude of the flux density is less than the magnitude with no eccentricity motion, which is more obvious at the extreme point. The rotor eccentricity will affect the performance of the motor.

5.2 Harmonic analysis of the air-gap flux density with the rotor eccentricity

For an obvious contrast of the air-gap flux-density distribution at different air-gap lengths, the Fourier's harmonic decomposition theory is used. If is used to decompose the air-gap flux-density harmonic under different rotor-eccentricity states. The fundamental wave, third-order harmonic and fifth-order harmonic of different air-gap lengths are calculated and compared as shown in Fig. 17.

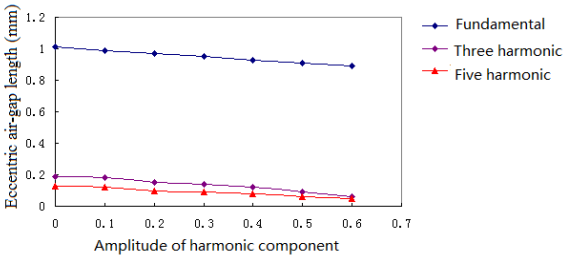

Figure 17. Harmonic-amplitude comparison with different eccentric lengths

As seen in Fig. 17, at an eccentric phenomenon appears, the value of the air-gap significantly affects the air-gap magnetic field. The maximum difference in the air-gap flux density at different positions can be increased by 20% when the rotor is eccentric. Besides, the maximal difference between the different positions of the air-gap will increase obviously when the eccentric magnitude of the rotor increases. Meanwhile, the third- and fifth-order harmonic of the air-gap magnetic field will appear at a certain change in an eccentric motion of the rotor of without affecting the fundamental magnetic field. The change in the harmonic is almost in accordance with the increase or decrease in the magnetic-field fundamental component.

6 CONCLUSIONS

The paper proposes a new compound-drive-type multi-degree-of-freedom permanent-magnet motor with a liquid suspension mode and discussing the motor basic structure and working principle. The analytical and 3D finite-element method are used to analyze the air-gap magnetic field of the motor in detail, and the results of comparative analysis verify the validity of the application of these two methods. A permanent-magnet rotor-eccentric magnetic-field model is set up and changes in the magnetic field due to the rotor eccentricity are analyzed along with the harmonic components of different air-gap lengths. The analysis results prove the correctness of the presented analysis and calculation methods. The future work will be towards optimization of the structural parameters.

ACKNOWLEDGMENT

This work is supported by the National Natural Science Foundation of China (No. 51577048, 51637001, 51407002, 51107031), the Natural Science Foundation of Hebei Province of China (No. E2018208155), the Overseas Students Science and Technology Activities Funding Project of Hebei Province (No. C2015003044), the National Engineering Laboratory of Energy-saving Motor & Control Technique, Anhui University.

REFERENCES

[1] Gregory S Chirikjian, David Stein. “Kinematic design and commutation of a spherical stepper motor”. *IEEE Trans. on Mechatronics*, 4, 4(1999), pp. 342–353.

[2] Huang, S, Tao X, Lin J. “The development of three-degree-of-freedom spherical motor”, *Electrical energy new technology*, 15, 2(1989), pp. 6-11.

[3] Li Z, Wang Q. “Research and development status of permanent magnet multidimensional spherical motor”, *Micro & special motor*, 34, 10(2006), pp. 7-11.

[4] K. Kahlen, R. W. DE Doncker. “Current regulators for multi-phase permanent magnet spherical machines”, *Proceedings of IEEE International Conference on Industrial Applications*, (2000), pp.2011-2016.

[5] B. Dehez, G. Galary, D. Grenier, B. Raucent. “Development of a spherical induction motor with two degrees of freedom”, *IEEE Transactions on Magnetics*, 42, 8(2006), pp.2077–2089.

[6] K. Davey, G. Vachtsevanos, R. Powers. “The analysis of fields and torques in spherical induction motors”, *IEEE Transactions on Magnetics*, 23, 1(1987), pp.273–282.

[7] Y. Liang, I. M. Chen, G. Yang, L. K.-M. Lee. “Analytical and experimental investigation on the magnetic field and torque of a permanent magnet spherical actuator”, *IEEE/ASME Transactions on Mechatronics*, 11, 4(2006), pp.409–419.

[8] K.-M. Lee, R. A. Sosseh, Z. Wei. “Effects of the torque model on the control of a VR spherical motor”, Control Engineering Practice, 12, 11(2004), pp.1437–1449.

[9] Li Z, Guo Z, Zhang Y. “Magnetic field analysis of a novel 3-DOF deflection type PM motor”, *Journal of Hebei University of Science and Technology*, 33, 5(2012), pp.422-428.

[10] Qiu Z, Li C, Zhou X, Zhang Y. “Analytical Calculation of No-Load Air-Gap Magnetic Field in Surface-Mounted Permanent Magnet Motors with Rotor Eccentricity”, *Transactions of China Electrotechnical Society*, 28, 3(2013), pp.115-121.

[11] Kong H, Liu J. “Study of rotor eccentricity effect on permanent magnet servo motor performance”, *Electric Machines and Control*, 20, 1(2016), pp.53-59.

[12] Li Z. “Robust control of PM spherical stepper motor based on neural networks”, *IEEE Transactions on Industrial Electronics*, 56, 8(2009), pp.2945-2954.

Zheng LI received his B.Sc. and Ph.D. degrees in electrical engineering and power electronics and electric drive from the Hefei University of Technology, Hefei, China, in 2002 and 2007, respectively. Since 2007, he has been a Lecturer, Associate Professor and Professor with the School of Electrical Engineering, Hebei University of Science and Technology. He is the author of more than 120 published papers. His current research interests include design, analysis and control of novel motors and actuators, intelligent control, and power electronics. He serves as an active reviewer for the IEEE Transactions on Industrial Electronics, IEEE Transactions on Energy Conversion, IEEE Transactions on Magnetics and Electric Power Components and Systems, etc.